JACS
JOURNAL OF THE AMERICAN CHEMICAL SOCIETY
pubs.acs.org/JACS

Open Access
This article is licensed under CC-BY 4.0

Article

Oxidation-State Control of Cobalt Electrocatalysts Enables Selective Hydrogenation of Nitrogen-Containing Aromatics

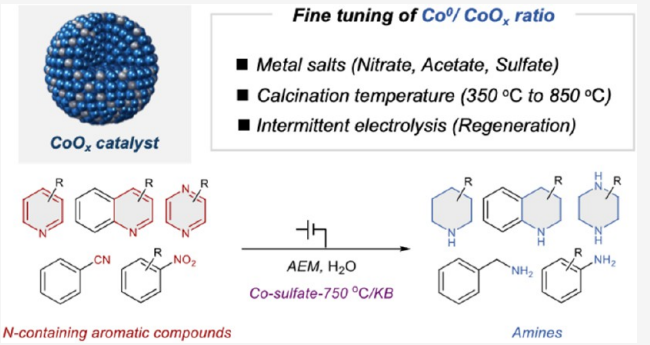
Akizumi Yonezawa, Yugo Shimizu, Juri Harada, Ryo Kurihara, Atsuki Hirama, Yusuke Muto, Reno Fukui, Ayaka Wakasugi, Koji Harano, Kazuhide Kamiya, Shoji Iguchi, Naoki Shida,* and Mahito Atobe*

Cite This: J. Am. Chem. Soc. 2026, 148, 48996–49009

Read Online

ACCESS | Metrics & More | Article Recommendations | Supporting Information

ABSTRACT: Electrocatalytic hydrogenation offers a sustainable route to reductive molecular transformations by generating hydrogen equivalents from water under ambient conditions. However, practical implementation requires earth-abundant heterogeneous electrocatalysts that combine activity, selectivity, and durability under operating conditions. Here, we report a highly selective electrocatalytic hydrogenation of nitrogen-containing aromatic compounds in an anion-exchange membrane electrolyzer using a carbon-supported cobalt catalyst with a finely tuned Co(0)/CoO_x ratio. The optimized catalyst, prepared from $CoSO_4 \cdot 7H_2O$ and calcined at 750 °C, converts pyridine to piperidine in >99% yield under ambient electrolysis conditions. Ex situ characterization and in situ Co K-edge X-ray absorption spectroscopy revealed that the catalyst retains an intermediate Co(0)/CoO_x ratio under reductive electrolysis conditions, whereas catalysts that become either excessively reduced or remain oxide-rich show lower activity. Kinetic analysis and density functional theory calculations indicate that pyridine hydrogenation proceeds through a Langmuir–Hinshelwood-type pathway, in which the mixed Co(0)/CoO_x surface provides an electronically suitable environment for pyridine adsorption and hydrogenation. This electronically tuned Co(0)/CoO_x surface enables selective hydrogenation of a broad range of nitrogen-containing aromatic compounds, including pyridines, quinolines, pyrazines, nitriles, and nitroarenes, while suppressing undesired hydrogenation pathways observed with Rh-based catalysts. Guided by the operando insight, intermittent electrolysis was introduced to prevent catalyst over-reduction during prolonged operation, enabling gram-scale conversion of pyridine to piperidine in 89% yield with stable cell voltage. These results highlight the importance of maintaining an intermediate Co(0)/CoO_x state for selective electrocatalytic hydrogenation with earth-abundant cobalt catalysts.



INTRODUCTION

The electrification of chemical synthesis is emerging as a central strategy for reducing the energy consumption and carbon footprint of the chemical industry.[1] Many industrially important transformations still rely on thermally driven processes that require elevated temperatures, high pressures, and stoichiometric chemical reductants or oxidants. In contrast, electrochemical synthesis enables redox transformations to be driven directly by electricity, ideally derived from renewable sources, while using electrons as clean reagents.[2−5] Among these transformations, electrocatalytic hydrogenation is particularly attractive because hydrogen equivalents can be generated in situ from water at the electrode surface, providing a sustainable alternative to conventional hydrogenation with pressurized H_2.[6−8] More recently, related electrochemical strategies have also attracted attention as efficient approaches for the incorporation of deuterium into organic molecules using D_2O as the deuterium source.[9−11]

For electrocatalytic hydrogenation to become a practical synthetic technology, the development of robust heterogeneous electrocatalysts is essential (Figure 1a). Homogeneous electrocatalysts, such as molecular mediators, offer precise molecular-level control over electron-transfer events, but their separation from reaction mixtures, recycling, and long-term use in process-oriented applications remain challenging.[12,13] Heterogeneous electrocatalysts, in contrast, can be directly integrated into flow electrolyzers and allow facile product separation and catalyst reuse.[14] These features make heterogeneous electrocatalysts particularly promising for the electrification of chemical manufacturing.

Received: June 14, 2026
Revised: September 18, 2026
Accepted: September 21, 2026
Published: September 29, 2026



ACS Publications
© 2026 The Authors. Published by American Chemical Society

https://doi.org/10.1021/jacs.6c12207
J. Am. Chem. Soc. 2026, 148, 48996−49009

Downloaded from pubs.acs.org/jacsat/article-pdf/148/45/48996/6703502/jacs.6c12207.pdf by NATL INST FOR MATLS SCIENCE (NIMS), Koji Harano on 18 November 2026

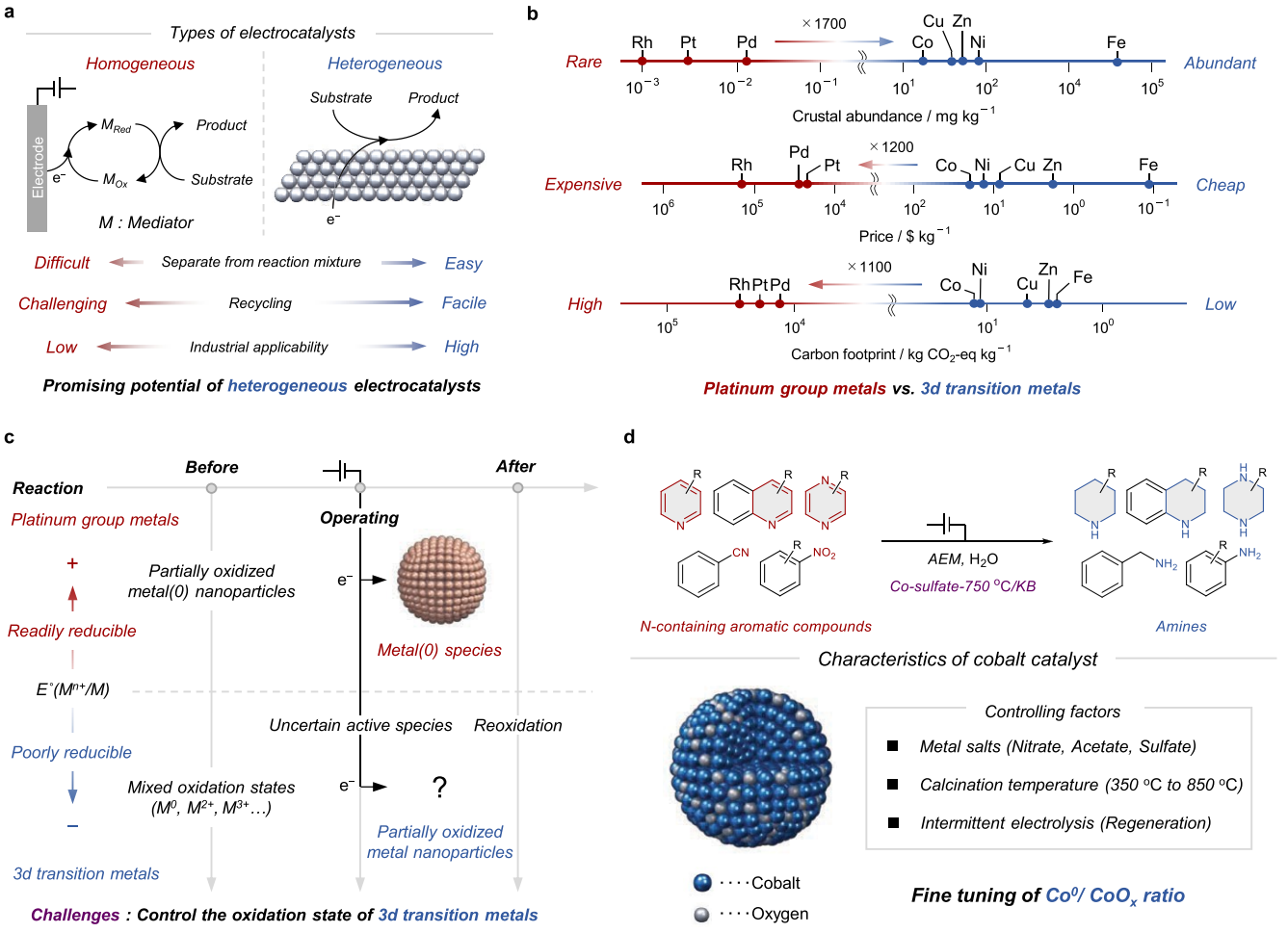


Figure 1. Background and concept of this work. (a) Comparison of homogeneous and heterogeneous electrocatalysts. (b) Comparison of platinum-group metals and 3d transition metals in terms of crustal abundance, price, and carbon footprint. (c) Schematic representation of the challenge in controlling the oxidation states of 3d transition-metal electrocatalysts. (d) Concept of this work.

Platinum-group metals (PGMs), including Rh, Pd, and Pt, have been widely used as heterogeneous hydrogenation catalysts because of their high activity and chemical robustness. However, their scarcity, high cost, and substantial environmental burden associated with mining and refining pose serious limitations for large-scale implementation (Figure 1b).[15−17] In comparison, earth-abundant 3d transition metals such as Fe, Co, Ni, Cu, and Zn offer clear advantages in terms of resource availability, price, and carbon footprint. Replacing PGMs with 3d transition metals is therefore a key objective in the development of sustainable electrocatalytic hydrogenation systems.[18−23]

Despite this promise, 3d transition-metal electrocatalysts present a fundamental challenge that is less pronounced for PGMs: their oxidation states can change dynamically before, during, and after electrolysis (Figure 1c). PGM nanoparticles are often converted under cathodic operation into relatively well-defined metal(0) species.[24] In contrast, 3d transition metals can exist as mixtures of metal(0), divalent, trivalent, or higher-valent oxide species, and their reducibility depends sensitively on the metal identity, local environment, electrolyte, pH, and applied potential.[25−27] As a result, the catalyst structure observed before or after electrolysis does not necessarily represent the true active state under operating conditions. This uncertainty makes it difficult to identify active species and to establish rational design principles for selective electrocatalytic hydrogenation using 3d transition metals.

We envisioned that this challenge could be addressed by deliberately controlling the balance between metallic cobalt and cobalt oxide species under electrocatalytic hydrogenation conditions (Figure 1d). Cobalt is particularly attractive because it combines earth abundance with hydrogenation activity, while its accessible redox chemistry offers an opportunity to tune the Co(0)/CoO_x ratio.[28] If appropriately controlled, the coexistence of metallic cobalt and cobalt oxide could generate an electronically balanced cobalt surface that facilitates both substrate adsorption and hydrogen transfer. However, achieving and maintaining such an optimal electronic state during prolonged cathodic electrolysis remains nontrivial.

Here we report a carbon-supported cobalt electrocatalyst that enables highly selective electrocatalytic hydrogenation of nitrogen-containing aromatic compounds in an anion-exchange-membrane (AEM) electrolyzer (Figure 1d). Nitrogen-containing aromatics were selected as target substrates because their hydrogenated derivatives are important structural motifs in pharmaceuticals, agrochemicals, dyes, and other fine chemicals.[29−33] Recent advances, including our previous work on Rh-catalyzed electrocatalytic pyridine hydrogenation in an AEM electrolyzer, have demonstrated the potential of electrocatalytic hydrogenation for this class of compounds using PGM catalysts.[9,34]

Earth-abundant metal electrocatalysts have also recently been developed for *N*-heteroarene hydrogenation. Cobalt-based

https://doi.org/10.1021/jacs.6c12207
J. Am. Chem. Soc. 2026, 148, 48996−49009

Downloaded from pubs.acs.org/jacsat/article-pdf/148/45/48996/6703502/jacs.6c12207.pdf by NATL INST FOR MATLS SCIENCE (NIMS), Koji Harano on 18 November 2026

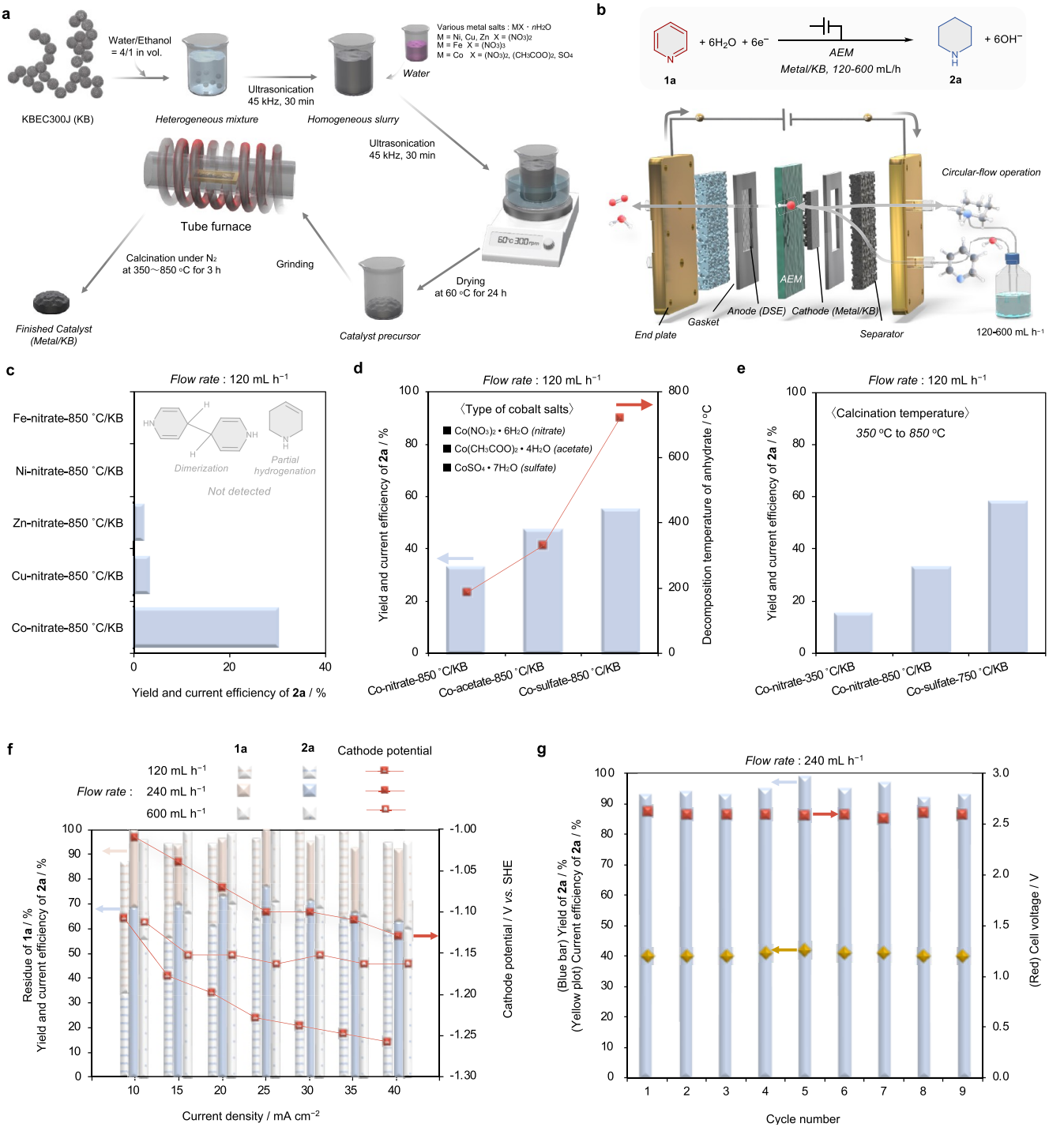


Figure 2. Preparation and evaluation of carbon-supported 3d transition-metal electrocatalysts for pyridine hydrogenation. (a) Preparation of Metal/KB catalysts by wet impregnation followed by thermal treatment under N_2. (b) Schematic illustration of electrocatalytic hydrogenation of pyridine (**1a**) to piperidine (**2a**) in an AEM electrolyzer equipped with a Metal/KB cathode and a DSE anode. (c) Initial screening of nitrate-derived 3d-metal catalysts calcined at 850 °C. (d) Effect of cobalt precursor on the electrocatalytic hydrogenation of **1a**. (e) Effect of calcination temperature on the catalytic performance of Co/KB catalysts. (f) Optimization of current density and catholyte flow rate using Co-sulfate-750 °C/KB. (g) Repeated electrolysis of **1a** using Co-sulfate-750 °C/KB.

systems have shown particularly promising performance for quinolines, which are relatively reactive *N*-heteroarenes.[35,36] More recently, a Ni-foam cathode enabled the hydrogenation of a broader range of aza-arenes, including pyridines, although acidic conditions were required.[37] Nevertheless, the selective electrocatalytic hydrogenation of less readily reducible *N*-heteroarenes such as pyridines using earth-abundant metals under neutral-to-alkaline conditions remains underdeveloped. Avoiding acidic conditions is particularly desirable for base-metal electrocatalysts because metal dissolution can compromise catalyst stability. In this work, we show that the Co(0)/CoO_x balance can be controlled through catalyst preparation and intermittent electrolysis, enabling broad substrate applic-

https://doi.org/10.1021/jacs.6c12207
J. Am. Chem. Soc. 2026, 148, 48996−49009

Downloaded from pubs.acs.org/jacsat/article-pdf/148/45/48996/6703502/jacs.6c12207.pdf by NATL INST FOR MATLS SCIENCE (NIMS), Koji Harano on 18 November 2026

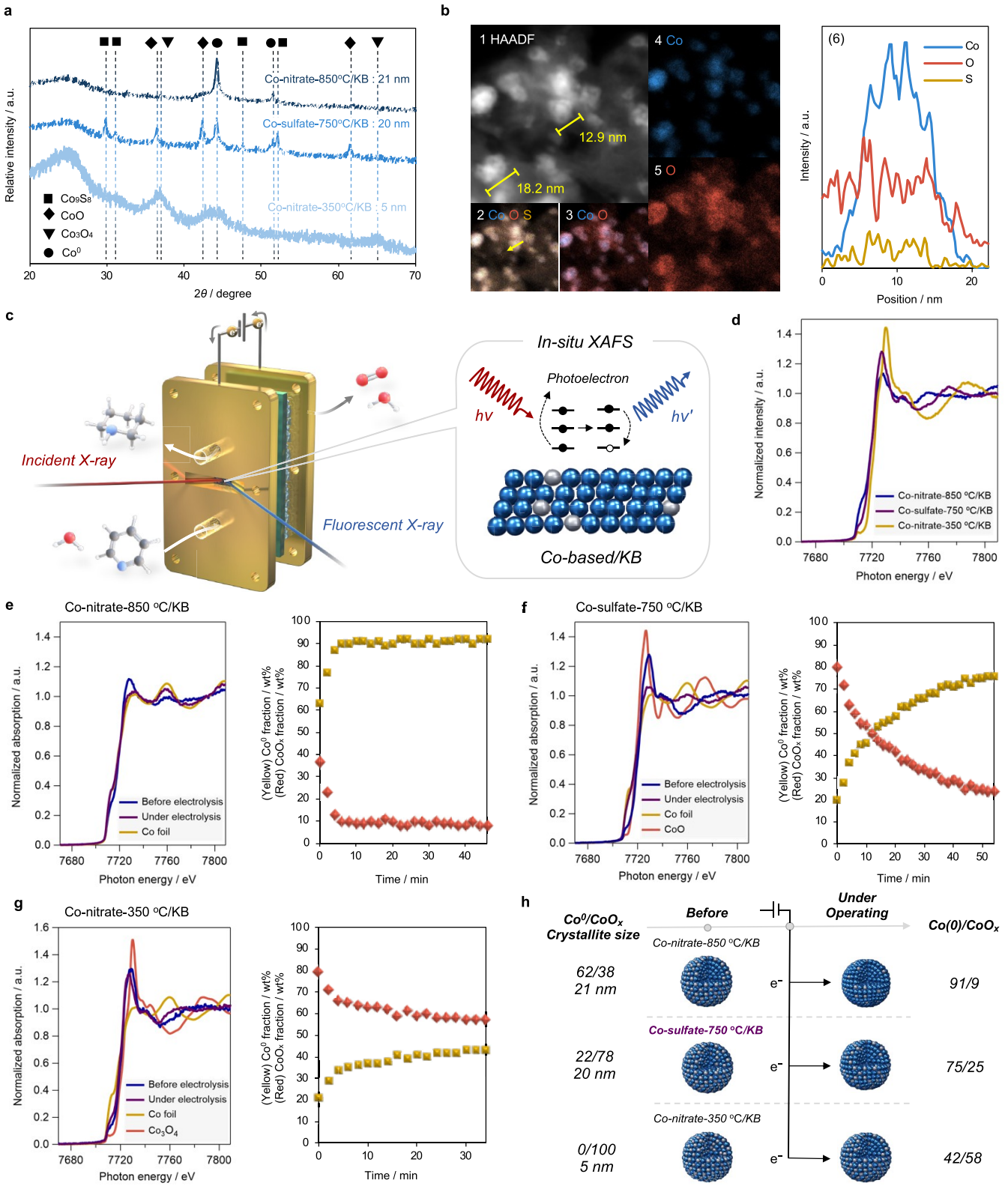


Figure 3. Structural and operando characterization of cobalt electrocatalysts. (a) XRD patterns of Co-nitrate-850 °C/KB, Co-sulfate-750 °C/KB, and Co-nitrate-350 °C/KB. (b) HAADF−STEM image, EDS elemental maps, and EDS line-scan profile of Co-sulfate-750 °C/KB. (c) Schematic illustration of the in situ Co K-edge XAFS measurement using an electrochemical cell equipped with an X-ray-transparent window. (d) Co K-edge XANES spectra of the three representative cobalt catalysts before electrolysis. (e−g) Co K-edge XANES spectra and time profiles of Co(0) and CoO_x fractions during electrolysis for (e) Co-nitrate-850 °C/KB, (f) Co-sulfate-750 °C/KB, and (g) Co-nitrate-350 °C/KB. (h) Summary of the structural and electronic-state changes of the three cobalt catalysts before and during electrocatalytic hydrogenation.

ability, high chemoselectivity, and gram-scale synthesis without relying on platinum-group metals or acid additives.

https://doi.org/10.1021/jacs.6c12207
J. Am. Chem. Soc. 2026, 148, 48996−49009

Downloaded from pubs.acs.org/jacsat/article-pdf/148/45/48996/6703502/jacs.6c12207.pdf by NATL INST FOR MATLS SCIENCE (NIMS), Koji Harano on 18 November 2026

RESULTS AND DISCUSSION

Preparation and Evaluation of Carbon-Supported 3d Transition-Metal Electrocatalysts

To identify earth-abundant electrocatalysts capable of promoting the hydrogenation of nitrogen-containing aromatic compounds, a series of carbon-supported 3d transition-metal catalysts were prepared by wet impregnation followed by thermal treatment under N_2 (Figure 2a, also see Supporting Information for details).[38] Metal salts were impregnated onto Ketjen black (KB) to give a metal loading of 20 wt %, and the resulting precursors were thermally treated at 350−850 °C to afford Metal/KB catalysts. Because 3d transition metals are readily oxidized in air and can undergo dynamic changes in oxidation state under cathodic operation, both the metal precursor and calcination temperature were considered key parameters for tuning the electronic state of the resulting catalysts.

The electrocatalytic hydrogenation of pyridine was performed in an AEM electrolyzer equipped with a membrane-electrode assembly using A201 membrane (Figure 2b). The A201 membrane has been demonstrated to exhibit excellent resistance to a broad range of organic solvents while retaining its electrochemical performance, making it well suited for organic electrosynthesis.[34,39,40] The Metal/KB catalyst layer was used as the cathode, while an oxygen-evolution DSE electrode served as the anode. Electrocatalytic hydrogenation of pyridine (**1a**) to piperidine (**2a**) was selected as a model reaction. In the cathode compartment, water serves as the source of hydrogen equivalents: electrochemical water reduction generates adsorbed hydrogen species (H_{ads}) on the catalyst surface, which subsequently react with adsorbed **1a** to form **2a**. The generated hydroxide ions migrate through the AEM and are oxidized at the anode to produce oxygen. The catholyte was circulated through the cathode compartment, allowing the mass transport of **1a** to the catalyst layer.

We first screened carbon-supported Fe, Co, Ni, Cu, and Zn catalysts prepared from the corresponding nitrate salts and calcined at 850 °C (Figure 2c). Electrolysis of an aqueous solution of **1a** at 25 mA cm^{-2} showed that Co-nitrate-850 °C/KB promoted the desired hydrogenation, affording **2a** in 30% yield after passage of 6 F mol^{-1} of charge. In contrast, the Fe-, Ni-, Cu-, and Zn-based catalysts prepared under the same nitrate-derived 850 °C conditions showed negligible activity, and **1a** was largely recovered. Neither partially hydrogenated pyridines nor dimerized products were detected by GC analysis (Figure S54), indicating that the major competing process was hydrogen evolution reaction (HER) rather than unselective substrate conversion. These results identified cobalt as the most promising metal component among the nitrate-derived 3d transition-metal catalysts examined under this initial screening condition. The activity of cobalt under these conditions may reflect an appropriate balance between substrate adsorption, hydrogen adsorption, and product desorption, in line with the Sabatier principle.[41]

We next examined the effect of the cobalt precursor on catalytic activity (Figure 2d). Cobalt catalysts were prepared from $Co(NO_3)_2{\cdot}6H_2O$, $Co(CH_3COO)_2{\cdot}4H_2O$, and $CoSO_4{\cdot}7H_2O$ under otherwise identical calcination conditions (see Supporting Information for the details of the thermal decomposition of these metal salts). The catalytic activity increased in the order nitrate < acetate < sulfate, and Co-sulfate-850 °C/KB afforded **2a** in 55% yield. This trend roughly followed the decomposition temperatures of the corresponding anhydrous cobalt salts, suggesting that the thermal decomposition behavior of the precursor influences the cobalt phase generated during calcination.[42−47]

The calcination temperature also had a pronounced effect on the catalytic performance (Figure 2e). Co-nitrate-350 °C/KB exhibited low activity, consistent with the formation of oxide-rich cobalt species. Co-nitrate-850 °C/KB showed improved activity, whereas Co-sulfate-750 °C/KB gave the highest yield among the catalysts examined in this comparison. These results show that the catalytic performance of cobalt-based electrocatalysts is strongly influenced by the precursor and calcination temperature. This dependence suggests that the structure and electronic state of cobalt generated during catalyst preparation play an important role in determining the hydrogenation activity, prompting us to conduct detailed structural and operando characterization of these catalysts.

Because the reaction involves competition between hydrogenation of **1a** and HER, the current density and catholyte flow rate were optimized using the best performing catalyst, Co-sulfate-750 °C/KB (Figure 2f). At a low flow rate of 120 mL h^{-1}, the supply of **1a** to the catalyst surface was insufficient, which likely promoted hydrogen evolution and decreased the current efficiency for **2a** formation. Increasing the flow rate improved substrate delivery and enhanced the efficiency of hydrogenation. Among the conditions examined, electrolysis at 25 mA cm^{-2} with a catholyte flow rate of 240 mL h^{-1} provided the best balance, affording **2a** in 77% yield after passage of 6 F mol^{-1} of charge. Under these conditions, the cathode potential was also less negative than those observed at lower flow rates, consistent with the suppression of excessive hydrogen evolution.

The durability of Co-sulfate-750 °C/KB was then evaluated by repeated electrolysis experiments (Figure 2g). When 14 F mol^{-1} of charge was passed to drive the reaction to completion, **2a** was obtained in greater than 90% yield over nine consecutive runs, with the maximum yield of 99%. The current efficiency remained above 40%, and no increase in cell voltage was observed during repeated operation (Figures S9−S10). These results demonstrate that Co-sulfate-750 °C/KB is a robust and reusable cobalt electrocatalyst for pyridine hydrogenation in the AEM electrolyzer, while also suggesting that its catalytically competent state can be maintained under the optimized electrolysis conditions.

Structural and Operando Characterization

To clarify why Co-sulfate-750 °C/KB exhibited the highest catalytic activity, we examined the structure and electronic state of representative cobalt catalysts by ex situ and in situ characterization (Figure 3). Three catalysts with distinct activities were selected for comparison: Co-nitrate-850 °C/KB, Co-sulfate-750 °C/KB, and Co-nitrate-350 °C/KB. This comparison allowed us to evaluate whether the catalytic performance was governed primarily by crystallite size, crystalline phase, or the electronic state of cobalt under operating conditions.

Powder X-ray diffraction (XRD) analysis revealed clear differences in the cobalt phases generated by the different preparation conditions (Figure 3a). Co-nitrate-850 °C/KB showed diffraction peaks assignable mainly to metallic Co, whereas Co-nitrate-350 °C/KB exhibited broad features consistent with oxide-rich cobalt species. In contrast, Co-sulfate-750 °C/KB contained metallic Co together with CoO and a minor Co_9S_8 phase.[48] Although Co_9S_8 was detected in the

Downloaded from pubs.acs.org/jacsat/article-pdf/148/45/48996/6703502/jacs.6c12207.pdf by NATL INST FOR MATLS SCIENCE (NIMS), Koji Harano on 18 November 2026

https://doi.org/10.1021/jacs.6c12207
J. Am. Chem. Soc. 2026, 148, 48996−49009

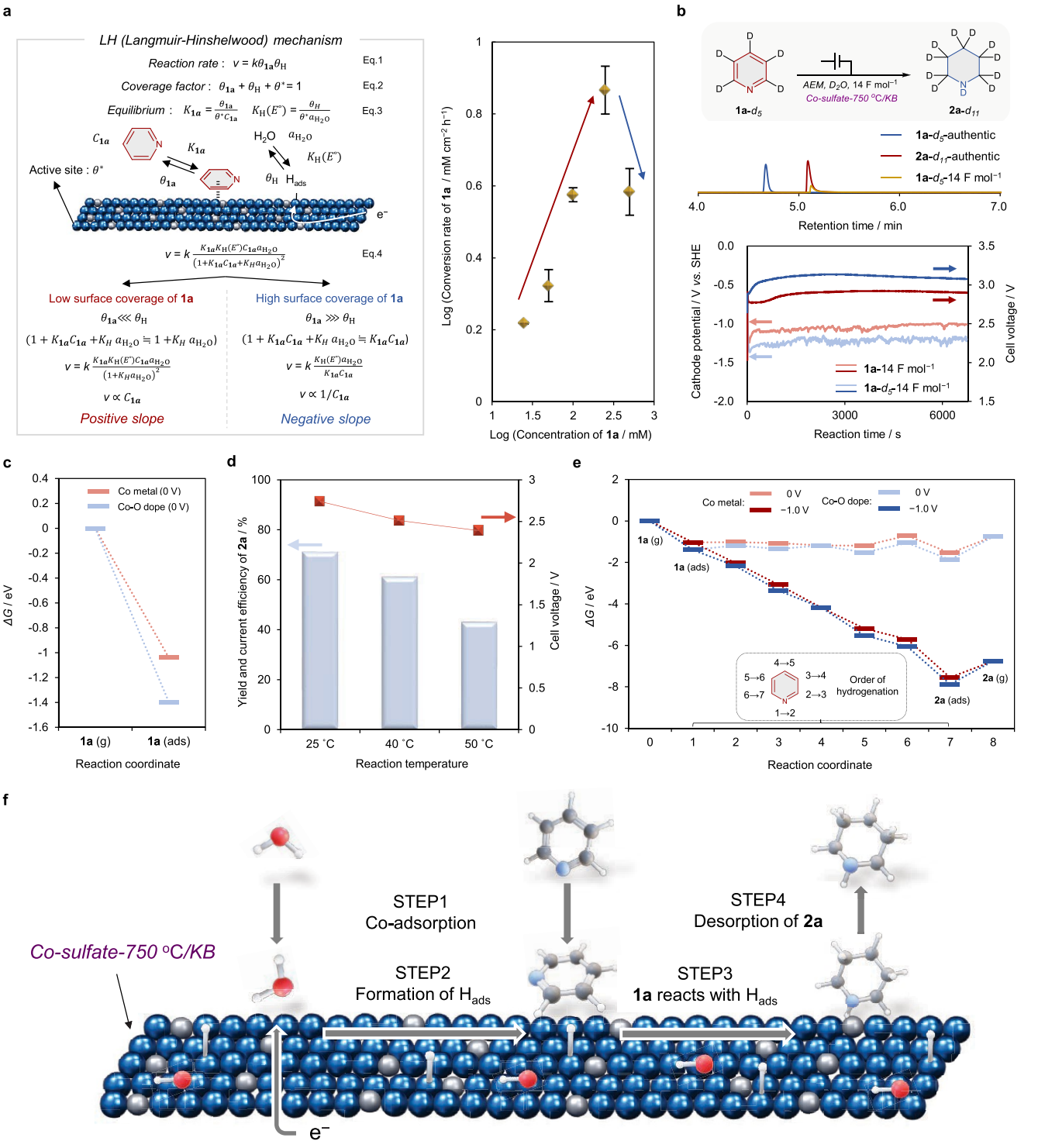


Figure 4. Mechanistic analysis of pyridine electrocatalytic hydrogenation on Co-sulfate-750 °C/KB. (a) Langmuir−Hinshelwood-type kinetic model and dependence of the conversion rate of **1a** on its concentration. (b) Deuterium-labeling experiment using **1a**-d_5 in D_2O and comparison of cathode potential and cell voltage with the nondeuterated reaction. (c) DFT-calculated adsorption free energies of **1a** on metallic cobalt and oxygen-doped cobalt surfaces. (d) Effect of reaction temperature on the yield and current efficiency of **2a** and cell voltage. (e) DFT-calculated free-energy profiles for stepwise hydrogenation of **1a** on metallic cobalt and oxygen-doped cobalt surfaces at 0 and −1.0 V. (f) Proposed reaction mechanism for electrocatalytic hydrogenation of **1a** to **2a** on Co-sulfate-750 °C/KB.

as-prepared Co-sulfate-750 °C/KB catalyst, the corresponding XRD and XPS features disappeared after electrolysis (Figures S13−S14).

This observation suggests that Co_9S_8 is transformed under the reductive electrolysis conditions. The crystallite sizes estimated by the Scherrer equation were similar for Co-nitrate-850 °C/KB and Co-sulfate-750 °C/KB, 21 and 20 nm, respectively. Notably, Co-nitrate-350 °C/KB, which showed the lowest catalytic activity, had the smallest crystallite size of approximately 5 nm. This result indicates that the activity trend cannot be explained simply by the exposed cobalt surface area. Rather, the cobalt phase and electronic state generated by the preparation

Downloaded from pubs.acs.org/jacsat/article-pdf/148/45/48996/6703502/jacs.6c12207.pdf by NATL INST FOR MATLS SCIENCE (NIMS), Koji Harano on 18 November 2026

https://doi.org/10.1021/jacs.6c12207
J. Am. Chem. Soc. 2026, 148, 48996−49009

conditions are likely key factors governing the catalytic performance.

The local morphology and elemental distribution of Co-sulfate-750 °C/KB were further examined by HAADF−STEM and EDS mapping (Figure 3b). The observed cobalt nanoparticles were approximately 10−20 nm in diameter, consistent with the crystallite size estimated from XRD. EDS mapping showed that oxygen was distributed around the cobalt-rich domains, and the line-scan profile revealed a relatively stronger cobalt signal in the particle interior and oxygen enrichment near the outer region. These observations support the formation of a core−shell-like structure consisting of a metallic cobalt-rich core and an oxide-rich surface layer.

Because the electronic state of 3d transition metals can change substantially under cathodic electrolysis, ex situ characterization alone is insufficient to identify the catalytically relevant state. We therefore conducted in situ Co K-edge XAFS using a custom-built electrochemical cell equipped with an X-ray-transparent window (Figure 3c). XANES spectra were collected for the three representative cobalt catalysts before and during electrolysis in the AEM electrolyzer (see Supporting Information for the detailed experimental and analytical procedures). The spectra before electrolysis were first compared with those of reference compounds and analyzed by linear-combination fitting (Figure 3d). Because Co K-edge XAFS provides bulk-averaged information on the cobalt electronic state, the $Co(0)/CoO_x$ fractions discussed below represent the average cobalt composition probed under the measurement conditions rather than the quantitative surface composition. The initial $Co(0)/CoO_x$ ratios were estimated to be 62/38 for Co-nitrate-850 °C/KB, 22/78 for Co-sulfate-750 °C/KB, and 0/100 for Co-nitrate-350 °C/KB, indicating that the cobalt species were partially or almost fully oxidized before electrolysis depending on the preparation conditions.

Under electrocatalytic hydrogenation conditions, all three catalysts underwent reduction, but the extent of reduction differed markedly (Figure 3e−g). Co-nitrate-850 °C/KB was rapidly reduced and reached a $Co(0)/CoO_x$ ratio of approximately 91/9 during electrolysis (Figure 3e). Co-sulfate-750 °C/KB was also reduced, but retained a larger fraction of CoO_x, reaching a $Co(0)/CoO_x$ ratio of approximately 75/25 under operating conditions (Figure 3f). In contrast, Co-nitrate-350 °C/KB remained oxide-rich even under cathodic operation, with a $Co(0)/CoO_x$ ratio of approximately 42/58 (Figure 3g). Thus, the three catalysts exhibit clearly distinct cobalt electronic states under reaction conditions, ranging from predominantly metallic to oxide-rich compositions.

The combined structural and operando analyses reveal that the highest activity of Co-sulfate-750 °C/KB is associated with an intermediate $Co(0)/CoO_x$ ratio under operating conditions rather than with crystallite size alone (Figure 3h). Co-nitrate-850 °C/KB, although similar in crystallite size to Co-sulfate-750 °C/KB, becomes predominantly metallic during electrolysis and shows lower activity. Co-nitrate-350 °C/KB remains too oxide-rich and is also less active. These results suggest that the coexistence of metallic Co and residual CoO_x is important for efficient pyridine hydrogenation. The intermediate $Co(0)/CoO_x$ balance observed for Co-sulfate-750 °C/KB is therefore associated with its high catalytic performance, possibly because the mixed cobalt state provides an electronic environment suitable for pyridine adsorption and hydrogenation.

Mechanistic Analysis of Pyridine Electrocatalytic Hydrogenation

To gain mechanistic insights into the electrocatalytic hydrogenation of pyridine on Co-sulfate-750 °C/KB, we first examined the dependence of the reaction rate on the concentration of **1a**. Because the reaction requires both adsorbed pyridine and adsorbed hydrogen species generated by electrochemical water reduction, we considered a Langmuir−Hinshelwood mechanism in which **1a** and H_{ads} are coadsorbed on the catalyst surface before hydrogen transfer (Figure 4a).[49,50] On the basis of this model, the reaction rate is expected to show a positive dependence on the concentration of **1a** when the surface coverage of **1a** is low, whereas excessive adsorption of **1a** should suppress the coverage of H_{ads} and lead to a negative dependence. Consistent with this expectation, the logarithmic plot of the conversion rate against the concentration of **1a** showed a positive slope at lower concentrations and turned over at higher concentrations. This behavior supports a surface-mediated hydrogenation pathway in which competitive adsorption of **1a** and H_{ads} governs the reaction rate.

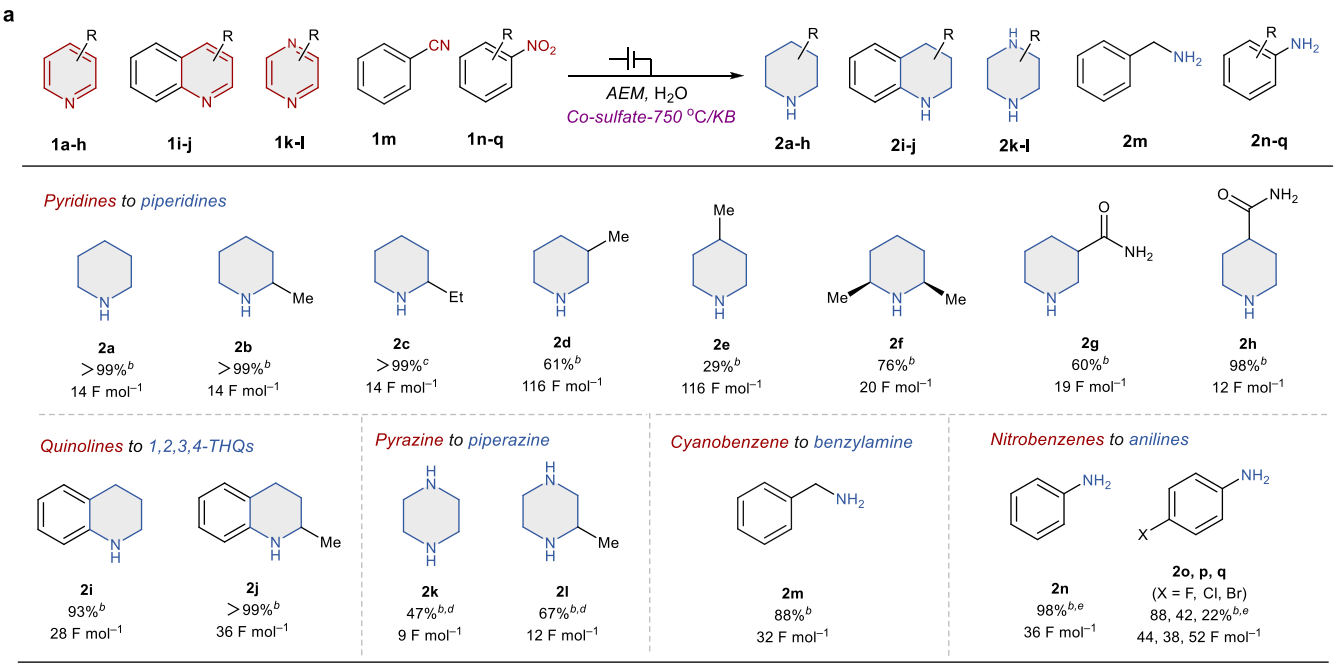
We next performed deuterium-labeling experiments to examine whether hydrogen transfer is involved in a kinetically relevant step (Figure 4b). Electrolysis of deuterated pyridine, **1a-d_5**, in D_2O afforded the corresponding deuterated piperidine, **2a-d_{11}**, as confirmed by GC−MS analysis using authentic samples. Compared with the electrolysis of nondeuterated **1a** in H_2O, the reaction using **1a-d_5**/D_2O required a more negative cathode potential and a higher cell voltage. This isotope-dependent change in electrochemical response suggests that the formation and/or transfer of adsorbed hydrogen species is involved in a kinetically relevant process during pyridine hydrogenation.

The role of residual cobalt oxide was then investigated by density functional theory (DFT) calculations. Guided by the in situ XAFS results, two model surfaces were considered: metallic cobalt and oxygen-doped cobalt, the latter serving as a simplified model for a cobalt surface containing residual oxide character (see Supporting Information for details). Adsorption of **1a** was more favorable on the oxygen-doped cobalt surface than on the metallic cobalt surface (Figure 4c). This result indicates that residual oxide species can stabilize adsorbed pyridine on the catalyst surface. Experimentally, increasing the reaction temperature from 25 to 50 °C resulted in a substantial decrease in the yield of **2a**, despite a decrease in cell voltage (Figure 4d). This temperature dependence is consistent with a reaction in which adsorption of **1a** plays an important role: higher temperature weakens substrate adsorption and decreases hydrogenation efficiency, while improving ionic conductivity and lowering the apparent cell voltage.

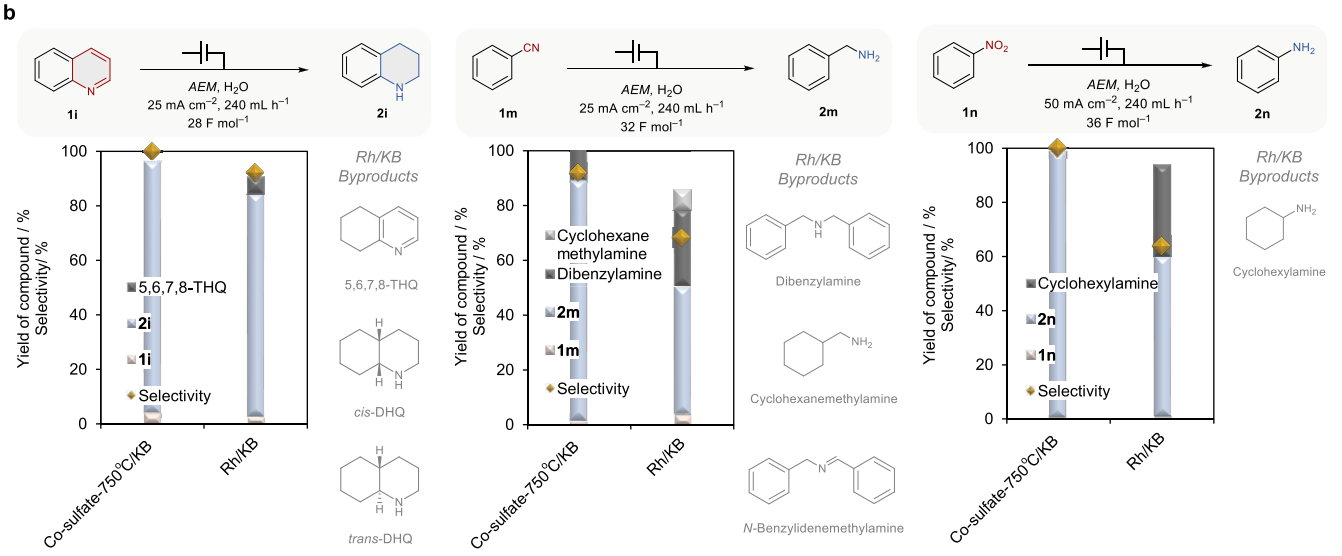
We further analyzed the hydrogenation sequence by calculating the free-energy profile for the stepwise hydrogenation of adsorbed **1a** (Figure 4e). At 0 V, several hydrogenation steps were thermodynamically uphill on both cobalt surfaces, indicating that purely thermal hydrogenation is unfavorable under these conditions. In contrast, when the applied potential was accounted for using the computational hydrogen electrode model at −1.0 V, the hydrogenation intermediates were substantially stabilized, and most elementary hydrogenation steps became energetically favorable except for product desorption. These results support the essential role of cathodic polarization in driving the dearomative hydrogenation of pyridine and are consistent with the experimental requirement for electrolysis. In addition, the calculated activation

Downloaded from pubs.acs.org/jacsat/article-pdf/148/45/48996/6703502/jacs.6c12207.pdf by NATL INST FOR MATLS SCIENCE (NIMS), Koji Harano on 18 November 2026

https://doi.org/10.1021/jacs.6c12207
J. Am. Chem. Soc. 2026, 148, 48996−49009



[a]Experimental conditions: catholyte, 5 mL solution of 100 mM substrate in water (**1a-h**,**1k-l**), MTBE (**1i-j**, **1m-q**); anolyte, air (for aqueous systems), 25 mM KOH + 75 mM K_2CO_3 (**1i-j**), 250 mM KOH + 750 mM K_2CO_3 (**1m**), 50 mM KOH + 50 mM K_2CO_3 (**1n-r**); current density, 25 mA cm^{-2} ; anode, DSE electrode; temperature, 25 °C. [b]Determined by GC. [c]Determined by ^1H NMR. [d]20 mA cm^{-2}, 40 °C. [e]50 mA cm^{-2}.



Experimental conditions: catholyte, 5 mL solution of 100 mM substrate in MTBE; anolyte, 25 mM KOH + 75 mM K_2CO_3 (**1i**), 250 mM KOH + 750 mM K_2CO_3 (**1m**), 50 mM KOH + 50 mM K_2CO_3 (**1n**); current density, 25 mA cm^{-2} (**1i** and **1m**), 50 mA cm^{-2} (**1n**); charge passed, 28 F mol^{-1} (**1i**), 32 F mol^{-1} (**1m**), 36 F mol^{-1} (**1n**), anode, DSE electrode; temperature, 25 °C.

Figure 5. Substrate scope and advantage of Co-sulfate-750 °C/KB catalyst compared to Rh/KB. (a) Substrate scope for the electrocatalytic hydrogenation of nitrogen-containing aromatic compounds using Co-sulfate-750 °C/KB. (b) Comparison of product yield and selectivity using Co-sulfate-750 °C/KB and Rh/KB as cathode catalysts.

barrier for water dissociation was higher on the O-doped Co surface than on pristine Co, suggesting that the beneficial role of residual oxide character is not attributable to facilitated water dissociation (Figures S33−35).

On the basis of these kinetic, isotope-labeling, and computational results, we propose the reaction mechanism shown in Figure 4f. Pyridine first adsorbs on the mixed Co(0)/CoO_x surface, whose electronically balanced state facilitates substrate adsorption. Electrochemical reduction of water then generates H_{ads} through the Volmer step, and sequential reaction of adsorbed pyridine with H_{ads} affords adsorbed piperidine.

Finally, piperidine desorbs from the catalyst surface to complete the catalytic cycle. The coexistence of metallic cobalt and residual cobalt oxide is proposed to generate a mixed Co(0)/CoO_x surface with an electronic state suitable for both pyridine adsorption and hydrogenation. This electronically balanced surface explains why Co-sulfate-750 °C/KB, which retains an intermediate CoO_x fraction under operating conditions, exhibits the highest catalytic activity.

https://doi.org/10.1021/jacs.6c12207
J. Am. Chem. Soc. 2026, 148, 48996−49009

Downloaded from pubs.acs.org/jacsat/article-pdf/148/45/48996/6703502/jacs.6c12207.pdf by NATL INST FOR MATLS SCIENCE (NIMS), Koji Harano on 18 November 2026

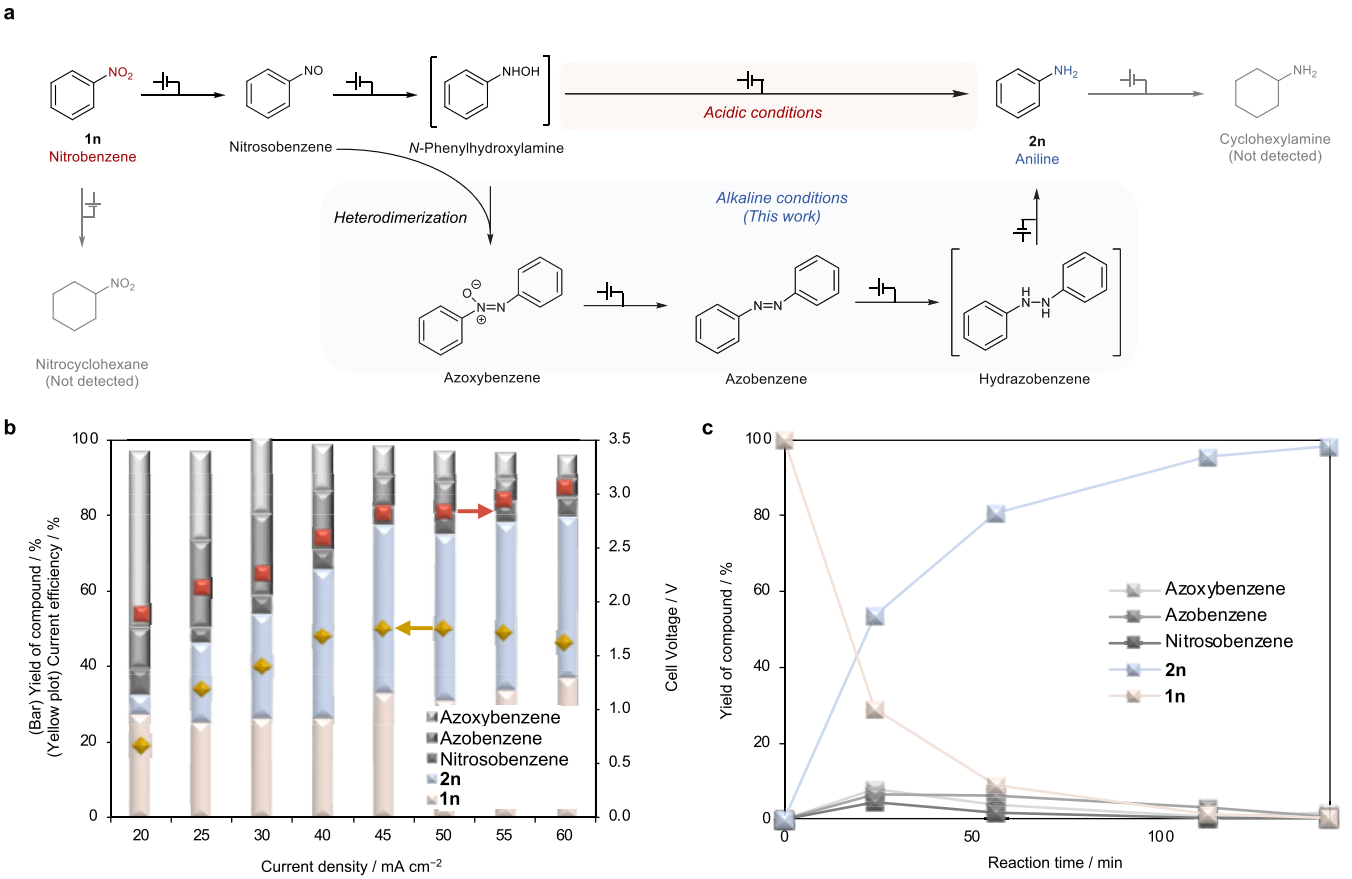


Figure 6. Electrocatalytic reduction pathway of nitrobenzene under AEM conditions. (a) Proposed reaction pathways for nitrobenzene hydrogenation under acidic and alkaline conditions. Under the alkaline AEM conditions used in this work, nitrosobenzene and *N*-phenylhydroxylamine can undergo heterodimerization to form azoxybenzene, followed by sequential reduction to azobenzene, hydrazobenzene, and aniline. (b) Effect of current density on the product distribution, current efficiency, and cell voltage for the electrocatalytic reduction of nitrobenzene. (c) Time-course profile for the electrocatalytic reduction of nitrobenzene to aniline.

Substrate Scope and Chemoselectivity

Having established the optimized cobalt electrocatalyst and its mechanistic features, we next examined the substrate scope of the electrocatalytic hydrogenation using Co-sulfate-750 °C/KB in the AEM electrolyzer (Figure 5a). In addition to non-substituted **1a**, substituted pyridines were also suitable substrates. 2-Methyl (**1b**) and 2-ethylpyridine (**1c**) afforded the corresponding 2-substituted piperidines in high yields, whereas 3- and 4-methylpyridines (**1d,e**) gave the desired products in more moderate yields and required a larger charge input.

Although the origin of this positional effect is not yet fully clear, the higher efficiency observed for 2-substituted pyridines may be related to facilitated desorption of the corresponding piperidines from the cobalt surface due to steric repulsion near the nitrogen atom. Lutidine (**1f**) and pyridinecarboxamides (**1g,h**) were also hydrogenated to the corresponding piperidine derivatives, indicating that the system tolerates both alkyl and amide substituents.

The applicability of the system was further demonstrated with fused and diazine substrates. Quinoline (**1i**) and 2-methylquinoline (**1j**) were selectively converted to 1,2,3,4-tetrahydroquinoline derivatives in high yields without detectable overhydrogenation of the benzene ring. This selectivity is notable because conventional hydrogenation of quinolines can suffer from over-reduction of the fused aromatic ring, especially with highly active PGM catalysts.[51,52] Pyrazines (**1k,l**) were also converted to the corresponding piperazines, demonstrating that the cobalt catalyst can promote hydrogenation of more electron-deficient diazine frameworks. Although cobalt-based thermal hydrogenation catalysts have been reported for *N*-heteroarenes such as pyridines and quinolines, such systems typically require molecular hydrogen and elevated temperature or pressure, highlighting the advantage of the present electrocatalytic system.[28]

Importantly, the present cobalt system was not limited to hydrogenation of heteroarenes. Cyanobenzene (**1m**) was reduced to benzylamine (**2m**) in high yield with only limited formation of dibenzylamine. Nitrobenzene (**1n**) was also converted to aniline (**2n**) in good yield. Halogenated nitrobenzenes (**1o−q**) were tolerated as well, providing the corresponding haloanilines (**2o−q**), although partial dehalogenation was observed for some substrates. The selectivity for haloaniline formation was improved under constant-voltage conditions, suggesting that careful control of the cathodic driving force is important for suppressing hydrodehalogenation (Figure S53).

Overall, the substrate-scope study highlights the distinctive chemoselectivity of Co-sulfate-750 °C/KB. The catalyst is sufficiently active to promote the hydrogenation of diverse nitrogen-containing aromatic compounds and reducible functional groups under ambient AEM conditions, yet it avoids the excessive hydrogenation often encountered with highly active PGMs. These results support the view that fine-tuning of the

Downloaded from pubs.acs.org/jacsat/article-pdf/148/45/48996/6703502/jacs.6c12207.pdf by NATL INST FOR MATLS SCIENCE (NIMS), Koji Harano on 18 November 2026

https://doi.org/10.1021/jacs.6c12207
J. Am. Chem. Soc. 2026, 148, 48996−49009

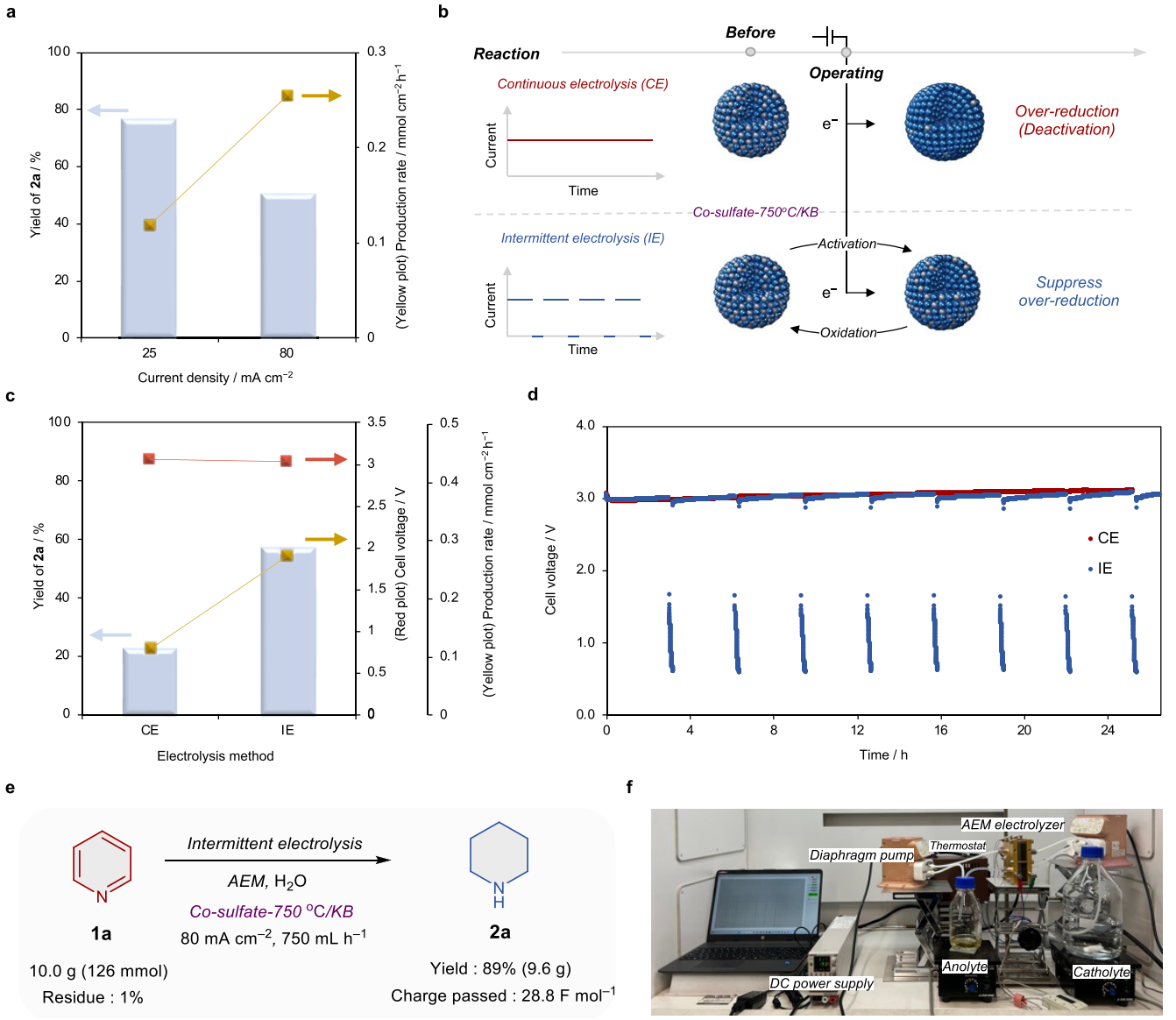


Figure 7. Gram-scale electrocatalytic hydrogenation enabled by intermittent electrolysis. (a) Effect of current density on the yield of **2a** and production rate using an enlarged cathode area. (b) Conceptual comparison of continuous electrolysis and intermittent electrolysis. Intermittent electrolysis suppresses over-reduction of Co-sulfate-750 °C/KB by periodically regenerating the partially oxidized cobalt surface. (c) Comparison of continuous electrolysis and intermittent electrolysis in terms of yield, cell voltage, and production rate. (d) Cell-voltage profiles during continuous and intermittent electrolysis. (e) Gram-scale electrocatalytic hydrogenation of **1a** to **2a** under intermittent electrolysis conditions. (f) Photograph of the AEM electrolysis setup used for gram-scale synthesis.

$Co(0)/CoO_x$ ratio provides not only high activity but also a practical means of controlling chemoselectivity in electrocatalytic hydrogenation.

Comparison of Co-Sulfate-750 °C/KB with Rh/KB

To further clarify the significance of Co-sulfate-750 °C/KB, control experiments were conducted using Rh/KB, which we previously reported as an effective electrocatalyst for the hydrogenation of nitrogen-containing aromatic compounds (Figure 5b). Quinoline (**1i**), benzonitrile (**1m**), and nitrobenzene (**1n**) were selected because Co-sulfate-750 °C/KB exhibited particularly high chemoselectivity for these substrates. The comparison was performed under identical reaction conditions except the catalyst (Co-sulfate-750 °C/KB: 20 wt %; Rh/KB: 27.6 wt %). Because the total catalyst loading on the electrode was fixed at 0.35 mg cm^{-2} for both catalysts, this difference is not expected to substantially affect the comparison.

For quinoline (**1i**), Co-sulfate-750 °C/KB selectively hydrogenated the *N*-containing ring to afford 1,2,3,4-tetrahydroquinoline (**2i**) in 93% yield with high selectivity. In contrast, Rh/KB produced a substantial amount of the regioisomeric 5,6,7,8-tetrahydroquinoline, arising from hydrogenation of the carbocyclic aromatic ring rather than the *N*-containing ring. Thus, the cobalt catalyst exhibits a pronounced preference for hydrogenation of the *N*-containing heteroaromatic ring, whereas Rh shows substantially lower ring selectivity.

A similarly clear difference was observed for benzonitrile (**1m**). Co-sulfate-750 °C/KB afforded benzylamine (**2m**) in 88% yield, with only a relatively small amount of dibenzylamine formed as a secondary product. In contrast, Rh/KB gave **2m** in moderate yield and produced a large amount of dibenzylamine.

Downloaded from pubs.acs.org/jacsat/article-pdf/148/45/48996/6703502/jacs.6c12207.pdf by NATL INST FOR MATLS SCIENCE (NIMS), Koji Harano on 18 November 2026

https://doi.org/10.1021/jacs.6c12207
J. Am. Chem. Soc. 2026, 148, 48996−49009

These results indicate that the cobalt catalyst more effectively suppresses secondary reactions of the initially formed benzylamine and thereby provides substantially higher selectivity toward the primary amine.

The most pronounced difference was observed for nitrobenzene (**1n**). Co-sulfate-750 °C/KB afforded aniline (**2n**) with essentially complete selectivity, whereas Rh/KB produced a substantial amount of cyclohexylamine through further hydrogenation of the aromatic ring. Thus, although Rh is highly active toward hydrogenation, its strong hydrogenation ability can lead to loss of chemoselectivity, whereas the cobalt catalyst selectively reduces the nitro group while preserving the aromatic ring.

Taken together, these comparisons demonstrate that the advantage of Co-sulfate-750 °C/KB over Rh/KB is not limited to the replacement of a precious metal with an earth-abundant catalyst. The cobalt catalyst exhibits distinct chemoselectivity across several classes of nitrogen-containing aromatic compounds: selective hydrogenation of the *N*-containing ring in quinoline, selective formation of a primary amine from benzonitrile, and selective nitro-group reduction without aromatic-ring hydrogenation. These results highlight the controlled hydrogenation ability of Co-sulfate-750 °C/KB as an important advantage over the more strongly hydrogenating Rh catalyst.

Nitrobenzene Reduction under AEM Conditions

The reduction of nitroarenes proceeded through a pathway distinct from the direct dearomative hydrogenation of pyridines and quinolines. Nitrobenzene (**1n**) was selected as a representative substrate to clarify this behavior (Figure 6). Under acidic hydrogenation conditions, nitrobenzene is generally reduced to aniline through nitrosobenzene and *N*-phenylhydroxylamine intermediates. In contrast, under alkaline conditions, nitrosobenzene and *N*-phenylhydroxylamine can undergo heterodimerization to form azoxybenzene, which is further reduced through azobenzene and hydrazobenzene before affording aniline (Figure 6a).[53] Because hydroxide ions are generated at the cathode during water reduction and transported through the AEM, the present electrolyzer provides a locally alkaline environment, making this condensation-mediated pathway plausible.

Consistent with this mechanistic picture, the product distribution strongly depended on the current density (Figure 6b). At lower current densities, partially reduced and coupled intermediates, including nitrosobenzene, azoxybenzene, and azobenzene, were observed in significant amounts. Increasing the current density promoted further reduction of these intermediates and increased the yield of aniline. At higher current densities, the cell voltage increased, providing a stronger cathodic driving force for the sequential reduction steps, and the current efficiency for aniline formation improved. These results indicate that, for nitrobenzene reduction, sufficient cathodic driving force is required not only for the initial reduction of the nitro group but also for the subsequent conversion of condensation-derived intermediates to aniline.

Time-course analysis under the optimized conditions further supported the sequential reduction pathway (Figure 6c). Nitrobenzene was rapidly consumed, while the amounts of nitrosobenzene, azoxybenzene, and azobenzene remained low throughout the reaction. Aniline accumulated steadily and became the dominant product at the end of electrolysis. These results show that, although nitrobenzene reduction proceeds through multiple intermediates under the alkaline AEM conditions, Co-sulfate-750 °C/KB can efficiently funnel these intermediates toward aniline without detectable overhydrogenation to cyclohexylamine. This behavior further highlights the moderate but productive hydrogenation ability of the cobalt catalyst, which enables functional-group reduction while suppressing excessive aromatic-ring hydrogenation.

Intermittent Electrolysis for Gram-Scale Reaction

Finally, we examined the scalability of the AEM electrocatalytic hydrogenation system using Co-sulfate-750 °C/KB. Because productivity becomes increasingly important upon scale-up, we first evaluated the effect of current density using an enlarged cathode area of 25 cm^2 (Figure 7a). The electrolysis was performed under continuous electrolysis (CE) conditions (Figure 7b, top). Increasing the current density from 25 to 80 mA cm^{-2} decreased the yield of **2a** but substantially improved the production rate. Thus, 80 mA cm^{-2} was selected for the subsequent scale-up study to prioritize space−time productivity while maintaining acceptable conversion efficiency.

When continuous electrolysis was performed under these high-current-density conditions, however, the yield of **2a** decreased markedly during prolonged operation (Figure 7c). On the basis of the in situ XAFS results, we attributed this decrease to over-reduction of Co-sulfate-750 °C/KB under sustained cathodic polarization. In CE condition, the catalyst surface is maintained under strongly reductive conditions for an extended period, which can shift the $Co(0)/CoO_x$ balance toward an excessively reduced state and diminish the beneficial contribution of residual cobalt oxide (Figure 7b). This interpretation is consistent with the lower activity of the overly reduced Co-nitrate-850 °C/KB catalyst observed in the preceding studies.

Intermittent electrolysis (IE) has been used to improve electrochemical processes such as pollutant removal, seawater electrolysis, and alcohol electrooxidation, where periodic current interruption can mitigate deactivation or regenerate active catalytic states.[54−56] To suppress this over-reduction, we introduced IE, in which short open-circuit periods were periodically inserted during the electrolysis (Figure 7b, bottom). During these pauses, partial reoxidation of the cobalt surface is expected to regenerate the catalytically competent $Co(0)/CoO_x$ state. Compared with continuous electrolysis, intermittent electrolysis substantially improved both the yield and production rate of **2a** under otherwise identical conditions (Figure 7c).

The cell voltage remained stable at approximately 3 V throughout the operation, and the periodic voltage drops during the current-off periods confirmed the programmed intermittent operation (Figure 7d). These results demonstrate that intermittent electrolysis is not merely an operational modification but a practical strategy for maintaining the optimal cobalt electronic state during prolonged electrocatalysis.

To further investigate the effect of intermittent electrolysis, operando XAFS measurements were performed after the electrolysis. As shown in Table S14, the reduced cobalt species gradually recovered toward a more oxidized state after the current was interrupted. This observation supports the hypothesis that intermittent electrolysis suppresses the gradual evolution toward a fully metallic cobalt state by allowing partial regeneration of the $Co(0)/CoO_x$ structure.

The optimized intermittent protocol was then applied to gram-scale pyridine hydrogenation (Figure 7e,f). Electrolysis of

Downloaded from pubs.acs.org/jacsat/article-pdf/148/45/48996/6703502/jacs.6c12207.pdf by NATL INST FOR MATLS SCIENCE (NIMS), Koji Harano on 18 November 2026

https://doi.org/10.1021/jacs.6c12207
J. Am. Chem. Soc. 2026, 148, 48996−49009

10.0 g of **1a** in 1 L of water using the 25 cm^2 AEM electrolyzer at 80 mA cm^{-2} and a catholyte flow rate of 750 mL h^{-1} afforded 9.6 g of piperidine (**2a**) in 89% yield after passage of 28.8 F mol^{-1} of charge. Only 1% of **1a** remained after electrolysis, indicating nearly complete conversion of the substrate. These results establish that the Co-sulfate-750 °C/KB-catalyzed AEM system can be translated from small-scale optimization to preparative-scale electrosynthesis while retaining high selectivity and operational stability.

CONCLUSION

In summary, we have developed a highly selective electrocatalytic hydrogenation system for nitrogen-containing aromatic compounds using a carbon-supported cobalt catalyst in an AEM electrolyzer. Among the 3d transition-metal catalysts examined, Co-sulfate-750 °C/KB exhibited the highest activity for pyridine hydrogenation, affording piperidine in high yield under ambient electrolysis conditions. Structural and operando analyses revealed that the catalytic performance is governed not simply by the presence of metallic cobalt but by the balance between Co(0) and CoO_x under reaction conditions. In situ Co K-edge XAFS showed that Co-sulfate-750 °C/KB retained an intermediate Co(0)/CoO_x ratio during electrolysis, whereas catalysts that became either excessively reduced or remained oxide-rich displayed lower activity.

Mechanistic studies further indicated that the Co(0)/CoO_x balance is critical for generating a cobalt surface suitable for pyridine adsorption and hydrogenation. Kinetic analysis supported a Langmuir−Hinshelwood-type surface reaction involving coadsorbed pyridine and H_{ads}, while DFT calculations showed that oxygen-containing cobalt surfaces stabilize adsorbed pyridine more strongly than metallic cobalt. Together, these findings indicate that the mixed Co(0)/CoO_x surface provides an electronically balanced environment for efficient pyridine hydrogenation, accounting for the high activity and selectivity of Co-sulfate-750 °C/KB.

The optimized AEM system was applicable to a broad range of nitrogen-containing aromatic compounds, including pyridines, quinolines, pyrazines, nitriles, and nitroarenes. Notably, the cobalt catalyst enabled selective formation of amines while suppressing overhydrogenation pathways often encountered with highly active noble-metal catalysts. Finally, intermittent electrolysis was introduced as a practical operational strategy to prevent over-reduction of the cobalt catalyst during prolonged electrolysis. This approach enabled gram-scale conversion of pyridine to piperidine in 89% yield with stable cell voltage.

These results establish fine-tuning of the Co(0)/CoO_x ratio as a key design principle for earth-abundant electrocatalysts in selective hydrogenation. More broadly, this work demonstrates that controlling the dynamic electronic state of 3d transition-metal catalysts under operating conditions can provide a powerful platform for the electrification of synthetic hydrogenation processes.

ASSOCIATED CONTENT

Supporting Information

The Supporting Information is available free of charge at https://pubs.acs.org/doi/10.1021/jacs.6c12207.

Description of the electrolyzer and experimental procedure, chromatography data, and ^1H NMR spectra (PDF)

AUTHOR INFORMATION

Corresponding Authors

Naoki Shida − *Department of Chemistry and Life Science, Yokohama National University, Hodogaya-ku, Yokohama 240-8501, Japan; PRESTO Japan Science and Technology Agency (JST), Kawaguchi, Saitama 332-0012, Japan; Institute of Advanced Sciences, Yokohama National University, Hodogaya-ku, Yokohama 240-8501, Japan;* orcid.org/0000-0003-0586-1216; Email: shida-naoki-gz@ynu.ac.jp

Mahito Atobe − *Department of Chemistry and Life Science, Yokohama National University, Hodogaya-ku, Yokohama 240-8501, Japan; Institute of Advanced Sciences, Yokohama National University, Hodogaya-ku, Yokohama 240-8501, Japan;* orcid.org/0000-0002-3173-3608; Email: atobe@ynu.ac.jp

Authors

Akizumi Yonezawa − *Department of Chemistry and Life Science, Yokohama National University, Hodogaya-ku, Yokohama 240-8501, Japan*

Yugo Shimizu − *Department of Chemistry and Life Science, Yokohama National University, Hodogaya-ku, Yokohama 240-8501, Japan*

Juri Harada − *Department of Chemistry and Life Science, Yokohama National University, Hodogaya-ku, Yokohama 240-8501, Japan*

Ryo Kurihara − *Research Center for Solar Energy Chemistry, Graduate School of Engineering Science, The University of Osaka, Toyonaka, Osaka 560-8531, Japan*

Atsuki Hirama − *Department of Chemistry and Life Science, Yokohama National University, Hodogaya-ku, Yokohama 240-8501, Japan*

Yusuke Muto − *Department of Chemistry and Life Science, Yokohama National University, Hodogaya-ku, Yokohama 240-8501, Japan*

Reno Fukui − *Department of Chemistry and Life Science, Yokohama National University, Hodogaya-ku, Yokohama 240-8501, Japan*

Ayaka Wakasugi − *Department of Chemistry and Life Science, Yokohama National University, Hodogaya-ku, Yokohama 240-8501, Japan*

Koji Harano − *Center for Basic Research on Materials, National Institute for Materials Science, Tsukuba, Ibaraki 305-0044, Japan; Research Center for Autonomous Systems Materialogy (ASMat), Institute of Integrated Research, Institute of Science Tokyo, Yokohama, Kanagawa 226−8501, Japan;* orcid.org/0000-0001-6800-8023

Kazuhide Kamiya − *Research Center for Solar Energy Chemistry, Graduate School of Engineering Science, The University of Osaka, Toyonaka, Osaka 560-8531, Japan; Innovative Catalysis Science Division, Institute for Open and Transdisciplinary Research Initiatives (ICS-OTRI), The University of Osaka, Suita, Osaka 565-0871, Japan;* orcid.org/0000-0002-6018-9277

Shoji Iguchi − *Graduate School of Engineering, Kyoto University, Kyoto 615-8530, Japan; PRESTO Japan Science and Technology Agency (JST), Kawaguchi, Saitama 332-0012, Japan;* orcid.org/0000-0002-2522-1358

Complete contact information is available at: https://pubs.acs.org/10.1021/jacs.6c12207

Downloaded from pubs.acs.org/jacsat/article-pdf/148/45/48996/6703502/jacs.6c12207.pdf by NATL INST FOR MATLS SCIENCE (NIMS), Koji Harano on 18 November 2026

Funding

This work was financially supported by JSPS KAKENHI Grant Numbers JP22K14541, JP23H04916 (Green Catalysis Science), JP23K23386, JP23K17370, JP24K01279. This work was supported by Japan Science and Technology Agency (JST) as a part of PRESTO program (JST Grant Nos. JPMJPR2373 and JPMJPR2471), and as part of Adopting Sustainable Partnerships for Innovative Research Ecosystem (ASPIRE) program, Grant Number JPMJAP2528.

Notes

The authors declare no competing financial interest.

■ ACKNOWLEDGMENTS

XRD, XPS, TEM, and NMR measurements were performed at the Instrumental Analysis Center (YNU). Part of this work was supported by the Electron Microscopy Unit, National Institute for Materials Science (NIMS). The authors thank Kouichi Okudaira (NIMS) for the assistance with HAADF-STEM and EDS experiments. The XAFS measurements were performed at the BL14B2 beamline of SPring-8 with the approval of the Japan Synchrotron Radiation Research Institute (JASRI) (Proposal Nos. 2024B1650, 2025B1646). DFT calculations were achieved through the use of SQUID at D3 Center, The University of Osaka.

■ REFERENCES

(1) International Energy Agency. Industry. https://www.iea.org/energy-system/industry (accessed Jan 15, 2026).

(2) Mallapragada, D. S.; Dvorkin, Y.; Modestino, M. A.; Esposito, D. V.; Smith, W. A.; Hodge, B.-M.; Harold, M. P.; Donnelly, V. M.; Nuz, A.; Bloomquist, C.; Baker, K.; Grabow, L. C.; Yan, Y.; Rajput, N. N.; Hartman, R. L.; Biddinger, E. J.; Aydil, E. S.; Taylor, A. D. Decarbonization of the Chemical Industry through Electrification: Barriers and Opportunities. *Joule* **2023**, *7* (1), 23−41.

(3) Xia, R.; Overa, S.; Jiao, F. Emerging Electrochemical Processes to Decarbonize the Chemical Industry. *JACS Au* **2022**, *2* (5), 1054−1070.

(4) Schiffer, Z. J.; Manthiram, K. Electrification and Decarbonization of the Chemical Industry. *Joule* **2017**, *1* (1), 10−14.

(5) Electrify to Decarbonize. *Nat. Catal.* 2023, *6* 12 1099 1100.

(6) Kleinhaus, J. T.; Wolf, J.; Pellumbi, K.; Wickert, L.; Viswanathan, S. C.; Junge Puring, K.; Siegmund, D.; Apfel, U.-P. Developing Electrochemical Hydrogenation towards Industrial Application. *Chem. Soc. Rev.* **2023**, *52* (21), 7305−7332.

(7) Akhade, S. A.; Singh, N.; Gutiérrez, O. Y.; Lopez-Ruiz, J.; Wang, H.; Holladay, J. D.; Liu, Y.; Karkamkar, A.; Weber, R. S.; Padmaperuma, A. B.; Lee, M.-S.; Whyatt, G. A.; Elliott, M.; Holladay, J. E.; Male, J. L.; Lercher, J. A.; Rousseau, R.; Glezakou, V.-A. Electrocatalytic Hydrogenation of Biomass-Derived Organics: A Review. *Chem. Rev.* **2020**, *120* (20), 11370−11419.

(8) Liu, C.; Wu, Y.; Zhao, B.; Zhang, B. Designed Nanomaterials for Electrocatalytic Organic Hydrogenation Using Water as the Hydrogen Source. *Acc. Chem. Res.* **2023**, *56* (13), 1872−1883.

(9) Bu, F.; Deng, Y.; Xu, J.; Yang, D.; Li, Y.; Li, W.; Lei, A. Electrocatalytic Reductive Deuteration of Arenes and Heteroarenes. *Nature* **2024**, *634* (8034), 592−599.

(10) Bu, F.; Deng, Y.; Lu, L.; Li, Y.; Song, W.; Yang, Z.; Luo, X.; Dong, X.; Yi, R.; Yang, D.; Wang, S.; Lei, A.; Li, W. Electrocatalytic Alkene Hydrogenation/Deuteration. *J. Am. Chem. Soc.* **2025**, *147* (7), 5785−5795.

(11) Ashikari, Y.; Mandai, K.; Yao, Y.; Tsuchihashi, Y.; Nagaki, A. Electrocatalytic Reduction of (Hetero)Aryl Halides in a Proton-exchange Membrane Reactor and Its Application for Deuteration. *ChemElectroChem* **2023**, *10* (23), No. e202300315.

(12) Costentin, C.; Robert, M.; Savéant, J.-M. Molecular Catalysis of Electrochemical Reactions. *Curr. Opin. Electrochem.* **2017**, *2* (1), 26−31.

(13) Francke, R.; Little, R. D. Redox Catalysis in Organic Electrosynthesis: Basic Principles and Recent Developments. *Chem. Soc. Rev.* **2014**, *43* (8), 2492−2521.

(14) Luque, R.; Burange, A. S.. *Heterogeneous Catalysis*; American Chemical Society: Washington, DC, USA, 2022.

(15) Clapson, M. L.; Durfy, C. S.; Facchinato, D.; Drover, M. W. Base Metal Chemistry and Catalysis. *Cell Rep. Phys. Sci.* **2023**, *4* (9), No. 101548.

(16) US Geological Survey. Leading Countries Based on the Mine Production of Titanium Minerals Worldwide in 2024; 2025.

(17) Torrubia, J.; Valero, A.; Valero, A. Energy and Carbon Footprint of Metals through Physical Allocation. Implications for Energy Transition. *Resour. Conserv. Recycl.* **2023**, *199* (107281), No. 107281.

(18) Sharifirad, A.; Michel, M.; Roge, V.; Lunca-Popa, P. Strategies for Enhancing the Electrocatalytic Performance of Transition Metal Thin Films Deposited via Chemical Vapor Process for Hydrogen Cells and Electrolysers. *ChemElectroChem* **2025**, *12* (7), No. e202400609.

(19) Maduraiveeran, G. Transition Metal Nanomaterial-Based Electrocatalysts for Water and CO2 Electrolysis: Preparation, Catalytic Activity, and Prospects. *Front. Energy Res.* **2024**, *12*, No. 1433103.

(20) Yang, Z.-G.; Xu, H.-M.; Shuai, T.-Y.; Zhan, Q.-N.; Zhang, Z.-J.; Huang, K.; Dai, C.; Li, G.-R. Recent Progress in the Synthesis of Transition Metal Nitride Catalysts and Their Applications in Electrocatalysis. *Nanoscale* **2023**, *15* (28), 11777−11800.

(21) Lakhan, M. N.; Hanan, A.; Hussain, A.; Ali Soomro, I.; Wang, Y.; Ahmed, M.; Aftab, U.; Sun, H.; Arandiyan, H. Transition Metal-Based Electrocatalysts for Alkaline Overall Water Splitting: Advancements, Challenges, and Perspectives. *Chem. Commun.* **2024**, *60* (39), 5104−5135.

(22) Anantharaj, S.; Aravindan, V. Developments and Perspectives in 3d Transition-metal-based Electrocatalysts for Neutral and Near-neutral Water Electrolysis. *Adv. Energy Mater.* **2020**, *10* (1), No. 1902666.

(23) Wu, G.; Zelenay, P. Activity versus Stability of Atomically Dispersed Transition-Metal Electrocatalysts. *Nat. Rev. Mater.* **2024**, *9* (9), 643−656.

(24) Nogami, S.; Shida, N.; Iguchi, S.; Nagasawa, K.; Inoue, H.; Yamanaka, I.; Mitsushima, S.; Atobe, M. Mechanistic Insights into the Electrocatalytic Hydrogenation of Alkynes on Pt−Pd Electrocatalysts in a Proton-Exchange Membrane Reactor. *ACS Catal.* **2022**, *12* (9), 5430−5440.

(25) Bard, A. J.; Parsons, R.; Jordan, J. *Standard Potentials in Aqueous Solution*; Routledge, 2017.

(26) Preikschas, P.; Zhang, J.; Seemakurthi, R. R.; Lian, Z.; Martín, A. J.; Xi, S.; Krumeich, F.; Ma, H.; Zhou, Y.; López, N.; Yeo, B. S.; Pérez-Ramírez, J. CO_2 Electroreduction to Long-chain Hydrocarbons on Cobalt Catalysts. *Adv. Energy Mater.* **2024**, *14* (47), No. 2401447.

(27) Bernal, M.; Bagger, A.; Scholten, F.; Sinev, I.; Bergmann, A.; Ahmadi, M.; Rossmeisl, J.; Cuenya, B. R. CO2 Electroreduction on Copper-Cobalt Nanoparticles: Size and Composition Effect. *Nano Energy* **2018**, *53*, 27−36.

(28) Murugesan, K.; Chandrashekhar, V. G.; Kreyenschulte, C.; Beller, M.; Jagadeesh, R. V. A General Catalyst Based on Cobalt Core−Shell Nanoparticles for the Hydrogenation of N-heteroarenes Including Pyridines. *Angew. Chem., Int. Ed.* **2020**, *59* (40), 17408−17412.

(29) Vitaku, E.; Smith, D. T.; Njardarson, J. T. Analysis of the Structural Diversity, Substitution Patterns, and Frequency of Nitrogen Heterocycles among U.S. FDA Approved Pharmaceuticals. *J. Med. Chem.* **2014**, *57* (24), 10257−10274.

(30) Marshall, C. M.; Federice, J. G.; Bell, C. N.; Cox, P. B.; Njardarson, J. T. An Update on the Nitrogen Heterocycle Compositions and Properties of U.s. Fda-Approved Pharmaceuticals (2013−2023). *J. Med. Chem.* **2024**, *67* (14), 11622−11655.

(31) Sridharan, V.; Suryavanshi, P. A.; Menéndez, J. C. Advances in the Chemistry of Tetrahydroquinolines. *Chem. Rev.* **2011**, *111* (11), 7157−7259.

Downloaded from pubs.acs.org/jacsat/article-pdf/148/45/48996/6703502/jacs.6c12207.pdf by NATL INST FOR MATLS SCIENCE (NIMS), Koji Harano on 18 November 2026

https://doi.org/10.1021/jacs.6c12207
J. Am. Chem. Soc. 2026, 148, 48996−49009

(32) Wells, G. M. Aniline. In *Handbook of Petrochemicals and Processes*; Routledge, 2018; pp 66−70.
(33) Heuer, L. Benzylamine. *Ullmann's Encyclopedia of Industrial Chemistry*; Wiley, July 15, 2006. DOI: 10.1002/14356007.a04_009.pub2.
(34) Shida, N.; Shimizu, Y.; Yonezawa, A.; Harada, J.; Furutani, Y.; Muto, Y.; Kurihara, R.; Kondo, J. N.; Sato, E.; Mitsudo, K.; Suga, S.; Iguchi, S.; Kamiya, K.; Atobe, M. Electrocatalytic Hydrogenation of Pyridines and Other Nitrogen-Containing Aromatic Compounds. *J. Am. Chem. Soc.* **2024**, *146* (44), 30212−30221.
(35) Guo, S.; Wu, Y.; Wang, C.; Gao, Y.; Li, M.; Zhang, B.; Liu, C. Electrocatalytic Hydrogenation of Quinolines with Water over a Fluorine-Modified Cobalt Catalyst. *Nat. Commun.* **2022**, *13* (1), No. 5297.
(36) Du, H.; Wang, T.; Li, M.; Yin, Z.; Lv, R.; Zhang, M.; Wu, X.; Tang, Y.; Li, H.; Fu, G. Identifying Highly Active and Selective Cobalt X-Ides for Electrocatalytic Hydrogenation of Quinoline. *Adv. Mater.* **2024**, *36* (41), No. e2411090.
(37) Dutta, S.; Narobe, R.; Waldvogel, S. R. Electrochemical Hydrogenation of Aza-Arenes Using H_2O as H Source. *J. Am. Chem. Soc.* **2026**, *148* (1), 2048−2058.
(38) Wang, B.; Li, T.; Qian, X.; Jin, L.; Yao, S.; Shen, X.; Qin, S. In Situ Growth of Co Nanoparticles in Ketjen Black for Enhanced Electrochemical Performances of Lithium-Sulfur Battery Cathode. *J. Solid State Electrochem.* **2021**, *25* (5), 1579−1590.
(39) Harada, J.; Yonezawa, A.; Muto, Y.; Wakasugi, A.; Fukui, R.; Shida, N.; Atobe, M. Evaluation of Durability of A201 Anion-Exchange Membranes towards Organic Solvents. *J. Solid State Electrochem.* **2025**, *29* (6), 2107−2114.
(40) Furutani, Y.; Shimizu, Y.; Harada, J.; Muto, Y.; Yonezawa, A.; Iguchi, S.; Shida, N.; Atobe, M. Electrocatalytic Oxidation of Primary Alcohols at the Triple-Phase Boundary in an Anion-Exchange Membrane Reactor with Nickel, Cobalt, and Iron Catalysts. *ACS Catal.* **2024**, *14* (11), 8922−8929.
(41) Ooka, H.; Huang, J.; Exner, K. S. The Sabatier Principle in Electrocatalysis: Basics, Limitations, and Extensions. *Front. Energy Res.* **2021**, *9*, No. 654460.
(42) Ehrhardt, C.; Gjikaj, M.; Brockner, W. Thermal Decomposition of Cobalt Nitrato Compounds: Preparation of Anhydrous Cobalt(II)-Nitrate and Its Characterisation by Infrared and Raman Spectra. *Thermochim. Acta* **2005**, *432* (1), 36−40.
(43) Gutiérrez-Martín, D.; Varela, A.; González-Calbet, J. M.; Matesanz, E.; Parras, M. Revisiting the Decomposition Process of Tetrahydrate Co(II) Acetate: A Sample's Journey through Temperature. *Appl. Sci.* **2022**, *12* (13), 6786.
(44) Kolta, G. A.; Askar, M. H. Thermal Decomposition of Some Metal Sulphates. *Thermochim. Acta* **1975**, *11* (1), 65−72.
(45) Małecka, B.; Łącz, A.; Drozdz, E.; Małecki, A. Thermal Decomposition of D-Metal Nitrates Supported on Alumina. *J. Therm. Anal. Calorim.* **2015**, *119* (2), 1053−1061.
(46) Wanjun, T.; Donghua, C. Mechanism of Thermal Decomposition of Cobalt Acetate Tetrahydrate. *Chem. Pap.* **2007**, *61* (4), 329−332.
(47) Ingraham, T. R.; Marier, P. The kinetics of the thermal decomposition of CoSO4 and Co3O4. *Thermochim. Acta* **1970**, *1* (1), 39−49.
(48) Wang, N.; Chen, B.; Qin, K.; Liu, E.; Shi, C.; He, C.; Zhao, N. Rational Design of Co9S8/CoO Heterostructures with Well-Defined Interfaces for Lithium Sulfur Batteries: A Study of Synergistic Adsorption-Electrocatalysis Function. *Nano Energy* **2019**, *60*, 332−339.
(49) Markunas, B.; Yim, T.; Snyder, J. PH-Mediated Solution-Phase Proton Transfer Drives Enhanced Electrochemical Hydrogenation of Phenol in Alkaline Electrolyte. *ACS Catal.* **2024**, *14* (22), 16936−16946.
(50) Lopez-Ruiz, J. A.; Sanyal, U.; Egbert, J.; Gutiérrez, O. Y.; Holladay, J. Kinetic Investigation of the Sustainable Electrocatalytic Hydrogenation of Benzaldehyde on Pd/C: Effect of Electrolyte Composition and Half-Cell Potentials. *ACS Sustainable Chem. Eng.* **2018**, *6* (12), 16073−16085.
(51) Bourriquen, F.; Hervochon, J.; Bartling, S.; Rockstroh, N.; Fischmeister, C.; Junge, K.; Beller, M. Teaching an Old Dog New Tricks: Simple Selective and Regiodivergent Quinoline Hydrogenation. *ACS Sustainable Chem. Eng.* **2023**, *11* (34), 12853−12858.
(52) Martinez-Espinar, F.; Blondeau, P.; Nolis, P.; Chaudret, B.; Claver, C.; Castillón, S.; Godard, C. NHC-Stabilised Rh Nanoparticles: Surface Study and Application in the Catalytic Hydrogenation of Aromatic Substrates. *J. Catal.* **2017**, *354*, 113−127.
(53) Lamy-Pitara, E.; N'Zemba, B.; Barbier, J.; Barbot, F.; Miginiac, L. Simple and Competitive Catalytic Hydrogenation of Nitrobenzene, Allyl Benzyl Ether and Benzyl Crotyl Ether in Alkaline Alcoholic Media. *J. Mol. Catal. A: Chem.* **1999**, *142* (1), 39−50.
(54) Kishimoto, N.; Kitamura, A. Effect of Intermittent Electrolysis on Electrolytic Removal of an Organic Pollutant. *J. Water Environ. Technol.* **2022**, *20* (5), 128−136.
(55) Sha, Q.; Wang, S.; Yan, L.; Feng, Y.; Zhang, Z.; Li, S.; Guo, X.; Li, T.; Li, H.; Zhuang, Z.; Zhou, D.; Liu, B.; Sun, X. 10,000-h-Stable Intermittent Alkaline Seawater Electrolysis. *Nature* **2025**, *639* (8054), 360−367.
(56) Li, Z.; Yan, Y.; Xu, S.-M.; Zhou, H.; Xu, M.; Ma, L.; Shao, M.; Kong, X.; Wang, B.; Zheng, L.; Duan, H. Alcohols Electrooxidation Coupled with H2 Production at High Current Densities Promoted by a Cooperative Catalyst. *Nat. Commun.* **2022**, *13* (1), No. 147.

Downloaded from pubs.acs.org/jacsat/article-pdf/148/45/48996/6703502/jacs.6c12207.pdf by NATL INST FOR MATLS SCIENCE (NIMS), Koji Harano on 18 November 2026